Journal of Sound and Vibration 577 (2024) 118339

Contents lists available at ScienceDirect

Journal of Sound and Vibration

journal homepage: www.elsevier.com/locate/jsvi

Decentralized modular semi-active controller for suppression of vibrations and energy harvesting

Dominik Pisarski *, Łukasz Jankowski

Institute of Fundamental Technological Research, Polish Academy of Sciences, Pawińskiego 5B, 02-106 Warsaw, Poland

ARTICLE INFO

Keywords:
Vibration control
Energy harvesting
Adaptive control
Semi-active control
Decentralized controller

ABSTRACT

The study investigates the problem of decentralized semi-active control of free vibration. The control scheme is designed for implementation in a modular controller architecture, where a collection of subcontrollers is employed, with each subcontroller being associated with a subsystem that represents a component of the vibrating structure. Each subcontroller uses state feedback from adjacent subsystem sensors to perform vibration suppression and energy harvesting using a switching control law. Furthermore, the assumption is made that neighbouring subcontrollers exchange information collaboratively to estimate the effects of coupling forces, achieving control efficiency comparable to that of a centralized approach. The effectiveness of the proposed approach is demonstrated on a modular suspension platform equipped with semi-active dampers and electromagnetic energy harvesters. The approach is evaluated under various free vibration scenarios, encompassing faulty measurement conditions, and is compared to passive and heuristic state-feedback control strategies. The results confirm that the proposed method attains a superior control performance, independent of the degree of decentralization in the adopted controller architecture, rendering it a viable solution for addressing large-scale semi-active control problems.

1. Introduction

The ever-increasing need for dependable and accessible structures and machinery has prompted engineers to explore innovative constructional solutions. Modular design, one of the most notable trends in modern engineering [1–3], has gained popularity due to its ease of assembly and maintenance, as well as its cost-effectiveness, making it highly desirable for wide range of applications. Modular structures are widely utilized in transportation systems, such as trains and trailers. Modularity is highly desirable in the automotive industry, as it provides synergies for multiple vehicle classes. Modular architectures are increasingly favoured in civil engineering, especially for slender buildings, temporary bridges, and tensegrity-based structures. Aerospace technology has also embraced modularity, particularly for satellites that require quick and uncomplicated assembly. Finally, modularity is a critical feature of smart factories in the context of "Industry 4.0", applied to the architecture of machinery and robotic platforms involved. The performance of a group of machines working together depends on their ability to engage in cooperative multitasking, which can be facilitated through flexible structural reconfiguration. In a smart factory setting, a modular architecture is highly desirable for conveyor belts, guideways, trolleys, and especially for robot manipulators that need to handle objects of varying sizes, shapes, and weights. To fully benefit from a modular structure, the integrated control system should have a similar modular architecture and operate in a decentralized manner.

* Corresponding author.
E-mail address: dpisar@ippt.pan.pl (D. Pisarski).

https://doi.org/10.1016/j.jsv.2024.118339
Received 25 March 2023; Received in revised form 28 December 2023; Accepted 7 February 2024
Available online 8 February 2024

List of symbols

S_k	Subsystem
C_k	Subcontroller
$\mathcal{G}_k$	Inter-connectivity set
g_{kj}	Boolean parameter
x_k	State vector
y_k	Extended state vector
u_k	Control input vector
u_{min}, u_{max}	Min and max admissible control value
n_k	Size of the state vector
m_k	Size of the control input vector
$A_k,\ B_{k,1}, \dots, B_{k,m_k}$	Subsystem matrices
$F_{k,j,r}$	Interaction force
$D_{k,j,r}$	Vector accommodating the interaction force
$r_{k,j}$	Total number of interaction forces acting on subsystem S_k from subsystem S_j
$\mathcal{A}_k,\ \mathcal{B}_{k,1}, \dots, \mathcal{B}_{k,m_k}$	Matrices of the extended subsystem
Q_k	Vibration damping/energy harvesting weighting matrix
P	Solution to the Lyapunov equation
$\bar{Q}_k$	Submatrix of Q_k collecting the entries corresponding to x_k
E_k	Energy-related function
T	Control time horizon
Δt	Sampling time
h_-	State measurement horizon
h_+	Control updating period
t'	Selected time instant for updating the interaction forces and control
$\tau_1, \dots, \tau_Z$	Sequence of time instants for updating the interaction forces and control
Z	Total number of time instants for updating the interaction forces and control
m	Module mass
k_b	Beam stiffness
k_s	Spring stiffness
k_u	Actuator stiffness coefficient
b_u	Actuator damping coefficient
R_h	Harvester resistance
L_h	Harvester inductance
k_t	Harvester mechanical–magnetic coupling constant
E_m	Mechanical energy
J_m	Mechanical energy integral
E_h	Harvested electrical energy

A decentralized, modular controller can be likened to a "plug-and-play" device that enables the smooth integration of a modular structure while maintaining its core features, such as ease of assembly, expansion, and reconfiguration. To ensure the modularity of the controller's architecture, the control algorithm implemented in subcontrollers associated with individual structural modules must meet two critical requirements. The first pertains to the quantity of state information utilized in the feedback control loops. Each subcontroller (control module) uses only the state measurement of its corresponding structural module, with the option to incorporate measurements from neighbouring modules that interact dynamically with the module in question. The second requirement is to ensure that each subcontroller employs an identical computational procedure. With these requirements met, adding or removing a subcontroller involves a straightforward plug-and-play action. Another significant advantage of the modular controller is its capacity for parallel computing, facilitating online updates and execution of control decisions. Additionally, the modular architecture of the controller is crucial for ensuring safety. In the event of a single computing unit malfunctioning or local measurement failures, the impact on the decisions of other subcontrollers is minimal. This significantly decreases the likelihood of the structure being driven to a hazardous state.

Decentralized controllers designed for structural control can be broadly categorized into two types [4]: those that use independent subcontrollers, often referred to as completely decentralized controllers, and those that incorporate a certain degree of collaboration among subcontrollers. The majority of the completely decentralized controllers have been developed based on the concept of isolated

subsystems that correspond to the segments of a vibrating structure. These controllers involve designing a set of state-dependent local control functions, where each subcontroller relies solely on the state information of its neighbouring subsystem. The concept of decomposing a structure into isolated subsystems and formulating local control laws using the linear–quadratic Gaussian (LQG) control methodology has been implemented for the purpose of active force control of large-scale slender buildings [5,6]. In this approach, the coupling forces between the subsystems are treated as external random disturbances. The LQG control technique has proven to be highly effective in scenarios where the building is subjected to earthquake excitation due to its ability to achieve optimality in the presence of disturbances characterized as additive white Gaussian noise. An analogous approach was employed to improve the positioning accuracy of a robotic manipulator [7]. The study presented in [8] introduced a decentralized control function based on polynomials for output-feedback control. The control parameters were optimized using a genetic algorithm. The efficacy of the proposed controller was examined through a case study involving a highway bridge under seismic excitations. The concept of isolated subsystems has also been extensively investigated in the context of decentralized structural semi-active control problems involving parametric control. Due to the nonlinearity introduced by the semi-active actuators and the size of the state vector, which may encompass hundreds degrees of freedom, the optimal control problem can be highly complex. Thus, rather than solving an intricate optimal control problem, it is often more practical to design heuristic local state-feedback functions with appropriate tuning to achieve the desired control performance. A local state-feedback controller was devised to mitigate the vibrations of cruise ships funnels [9]. This control system utilizes a set of semi-active dampers operating independently, with each damper being controlled via the skyhook method [10]. A decentralized state-feedback control can be established utilizing the prestress-accumulation release principle [11], with the aim of transferring vibrational energy from lightly-damped low-order modes to high-frequency modes where it can be effectively dissipated by material damping mechanisms. This approach has been validated on a frame structure equipped with semi-active lockable joints [12]. The development of decentralized state-feedback control functions can also be achieved through a specially designed structural model [13]. In this approach, the authors proposed discretizing the continuous problem described by the bilinear partial differential equation using the Galerkin method with a specially selected subspace onto which the solution to the dynamical equation is projected. It was shown that the proper choice of the basis for this subspace and the optimization of the resulting model's mass and stiffness matrices ensure that the assumed switching control law can operate using only local state information. The effectiveness of the proposed decentralized controller was demonstrated through experiments conducted on a vibrating semi-active span structure equipped with a set of actuators with controlled damping and stiffness parameters.

While fully decentralized controllers are commonly employed due to their practicality, their effectiveness may be limited in complex systems with broad frequency ranges of vibration. In these cases, the uncoordinated operation among subcontrollers aimed at mitigating vibrations at the actuator positions within the structure may result in the constant transmission of vibration energy between different points of the structure, resulting in inadequate overall stabilizing performance. This phenomenon was thoroughly analysed in [14], where it was demonstrated that even for a relatively simple system comprising a cantilever structure with semi-active elastomer-based actuators, isolating subcontrollers with limited state information may significantly reduce stabilizing performance when higher vibration modes are present. Collaborative decentralized controllers, in contrast to fully decentralized controllers, employ a communication network to facilitate the exchange of information between subcontrollers regarding the state of their adjacent subsystems. The purpose of this cooperative control is to provide efficiency levels comparable to centralized controllers that rely on global state information. In [15], the authors investigated the effects of exchanging varying amounts of state information on the stabilizing performance of decentralized controllers. To achieve this, they proposed partitioning a structure into a collection of overlapping subsystems (see also [16]). Each subsystem was then operated by an individual subcontroller designed using the linear–quadratic regulator (LQR) technique. The amount of state information exchanged between the subcontrollers was proportional to the degree of overlap between the subsystems. Through extensive numerical experiments involving a high-rise building model, it was validated that increasing the amount of exchanged state information resulted in the decentralized controller approaching the performance level of the centralized LQR controller. A similar finding was reported in [17], where the authors applied the concept of overlapping subsystems and the LQG control design to mitigate vibration in a cable-stayed bridge. An alternative collaborative decentralized strategy for active structural control, utilizing LQR design, was proposed in [18]. The authors incorporated a sparsity cost function, combined with an energy-related objective function, to achieve the desired structure for the stabilizing state-feedback control function, which is obtained by solving the Riccati equation. The effectiveness of this decentralized approach was evaluated through a study on a multi-storey building. Collaborative decentralized controllers have also proven to be effective in semi-active structures. In [19], it was demonstrated that cooperative control can be effectively employed to enhance the trajectory of a load traversing over a carrying structure supported by magneto-rheological supports. The author proposed utilizing a set of subcontrollers that operate based on energy-related vibration metrics. These metrics are estimated through a distributed averaging protocol, which necessitates a circular network for communication among the subcontrollers. The superior stabilizing performance of the collaborative decentralized controller was also confirmed for the cantilever beam structure equipped with semi-active damping blocks [20]. The study involved the development of a decentralized state-feedback switching control law based on the solution to the finite horizon optimal control problem. One of the critical parameters of this control law is the matrix that provides the ability to adjust the amount of state information employed by the local subcontrollers, following the assumed communication network characteristics.

Regardless of controller structuring, recent advancements in the development of active and semi-active control devices have resulted in numerous innovative control methods, in particular those leveraging soft computing algorithms, facilitating efficient adjustment of control decisions in scenarios where the structural model is incomplete or the system operates under permanently changing excitation. In [21], a neural network based algorithm was developed to control flexible cantilever plates equipped

with piezoelectric sensor–actuator pairs and subject to unknown periodic and random excitation. The neurocontroller employs a set of emulator neural networks which are also trained to forecast the future response of the structure. The study presented in [22] introduced the controller for a semi-active tuned liquid wall damper using an ensemble of recurrent neural networks. The method confirmed high performance is stabilizing the vibration of a multi-storey building exposed to wind and seismic hazards. A floating fuzzy logic based algorithm was developed for controlling structures equipped with magnetorheological dampers [23]. This algorithm enables the updating of control inputs to accommodate various types of loading and changes in the structural model, including the incorporation of nonlinearities. A neuro-fuzzy logic controller was designed to control the parameters of magnetorheological elastomers, aiming to mitigate the vibrations on offshore platforms [24]. This method enables the adaptation of control decisions to address irregular wave-induced excitations. In the group of controllers that allows adapting the control decision to changing environmental conditions, recent attention has been distinctly directed towards methodologies grounded in reinforcement learning (RL) algorithms. In [25], three reinforcement learning (RL) algorithms – specifically, policy gradient actor-critic, temporal-difference, and value function approximation – were investigated within the context of stabilizing a benchmark cart–pole system, with no prior information regarding its parameters. The Q-learning RL algorithm was developed to tune a fuzzy-PD controller to reduce the vibration of a high-rise building [26]. This method was successfully tested for seismic excitation. In [27], the RL actor-critic algorithm was implemented to stabilize a swinging chain. This algorithm enabled the optimization of control decisions using incomplete state information. The actor-only RL-based algorithm was developed to approximate the optimal switching pattern for operating magnetorheological dampers [28]. The method was implemented on a simply supported beam subjected to unknown periodic excitation.

In this paper, we propose a decentralized collaborative controller to control the free vibration of semi-active structures. The approach is predicated upon the partitioning of the structure in a manner that culminates in a collection of dynamically interacting subsystems, with each being operated by a dedicated subcontroller. Relative to prior research, the primary novel contribution of this work is rooted in the foundational presumption of the control system's modularity. In light of this, our objective is to devise a novel control algorithm that ensures the uniform operation of each subcontroller within the controller's network. In pursuit of suboptimal performance, the algorithm computes and incorporates the dynamical model of interactions among neighbouring subsystems, which is actualized through the collaborative efforts of subcontrollers, who exchange essential state information. Additionally, given that the control objective encompasses both vibration mitigation and energy reaping, the devised control law incorporates a tunable parameter to attain the desired trade-off between these competing aims. The effectiveness of the control is evaluated through the utilization of a purpose-built experimental setup featuring a modular suspension system. The study presents a comprehensive analysis of the control performance evaluated through various decentralized controller architectures, while also drawing comparisons with both the centralized solution and the alternative decentralized strategy based on isolated subsystems [14].

The organization of the subsequent sections of this paper is as follows: Section 2 presents the fundamental concepts and definitions of the modular system that incorporates a decentralized collaborative controller. In Section 3, we formulate and solve the problem of decentralized control, providing a comprehensive methodology for designing interaction forces and a computational algorithm for updating control decisions. Section 4 evaluates the performance of the designed controller through experiments conducted on a modular suspension platform. Finally, in Section 5, we summarize the findings.

2. The investigated system

This work studies a class of semi-actively controlled vibrating structures that can be represented as a set of dynamically interacting subsystems (see Fig. 1) $S_k(x_k)$, $k = 1, \dots, K$, with the internal state vector $x_k(t) = [x_{k,1}(t), \dots, x_{k,n_k}(t)]^T : [0,T] \to \mathbb{R}^{n_k}$ defined for time $t \in [0,T]$, where $T > 0$ refers to a considered control time. Each subsystem's vector x_k combines structural state variables (generalized displacements and velocities) with variables that characterize integrated energy harvesting devices (e.g. displacements, velocities, and electric currents in the case of electromagnetic devices [29]). The interactions between subsystems are defined by the inter-connectivity sets:

$$\mathcal{G}_k = \{j : \ g_{kj} = 1\}, \ \ k = 1, \dots, K, \tag{1}$$

where g_{kj} is a Boolean parameter given by $g_{kj} = 1$ if the subsystem S_k is dynamically coupled with the subsystem S_j and $g_{kj} = 0$ otherwise. For each subsystem $S_k(x_k)$ we associate a subcontroller $C_k(u_k)$ with the control input vector $u_k(t) = [u_{k,1}(t), \dots, u_{k,m_k}(t)] : [0,T] \to \mathcal{U}$. The set of admissible controls is assumed to be bounded by the minimum and the maximum values $u_{min} < u_{max}$ that correspond to the physical constraints of a semi-active device (e.g. extreme voltages), i.e., $\mathcal{U} = [u_{min}, u_{max}]^{m_k} \subset \mathbb{R}^{m_k}$. The dynamics of each subsystem $S_k(x_k)$, $k = 1, \dots, K$, is characterized by the ordinary bilinear differential equation:

$$\dot{x}_k(t) = A_k \, x_k(t) + \sum_{i=1}^{m_k} u_{k,i}(t) \, B_{k,i} \, x_k(t) + \sum_{j \in \mathcal{G}_k} \sum_{r=1}^{r_{k,j}} D_{k,j,r} \, F_{k,j,r}(t), \ \ x_k(0) = x_k^0. \tag{2}$$

In (2), the constant matrices A_k and $B_{k,i}$ with dimensions $n_k \times n_k$ define the internal subsystem's dynamics (coupling the structural states with the states of the integrated energy harvesting devices) and the influence of the ith semi-active device, respectively. The constant vectors $D_{k,j,r}$ with dimensions $n_k \times 1$, $j \in \mathcal{G}_k$ and $r = 1, \dots, r_{k,j}$ (with $r_{k,j}$ being the total number of interaction forces acting on subsystem S_k from subsystem S_j), accommodate the interaction forces $F_{k,j,r}$ into the system dynamics. They are constructed based on the principle that $D_{k,j,r}$ has an entry equal to 1 in the row corresponding to the element of the vector x_k subjected to force $F_{k,j,r}$, and all other entries are equal to 0. The interaction forces $F_{k,j,r} = F_{k,j,r}(t) : [0,T] \to \mathbb{R}$, $j \in \mathcal{G}_k$, are assumed to be bounded and piecewise continuous functions. The initial conditions are assumed to be $x_k^0 \neq 0$ for free-vibration scenarios.

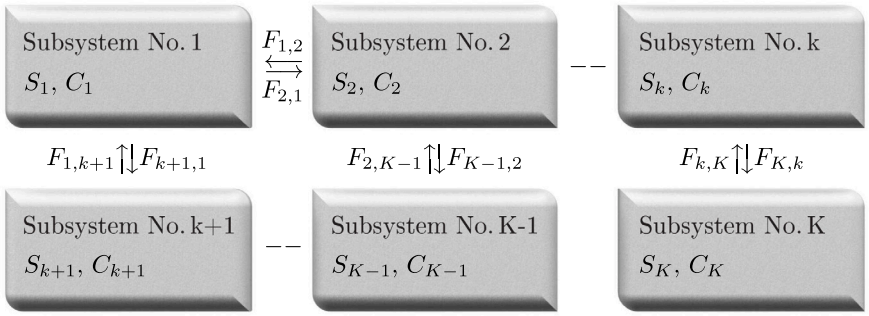

Fig. 1. Semi-active vibrating structure represented as a set of dynamically interacting subsystems. In the depicted arrangement, the inter-connectivity set for the subsystem S_1 is given by $\mathcal{G}_1 = \{2, k+1\}$.

The bilinear dynamical Eq. (2) can approximate the behaviour of diverse structural control systems incorporating various types of semi-active devices. In addition to established solutions involving magnetorheological dampers – such as those employed in vehicular suspensions [30] or span structures [31,32] – or tuned mass damper that are widely implemented in high-rise buildings [33], the analysed dynamical system is also adaptable to new-emerging smart materials that enable efficient control of both damping and stiffness parameters. In particular, magnetorheological elastomers, with their unique physical properties and structural flexibility (allowing, for example, the construction of radial-chain [34] or X-shaped structures [35]), offer responsive control over the viscoelastic parameters. Structural control problems have also stimulated the advancements in dielectric materials [36] and magnetoactive elastomers [37]. The former facilitates effective stiffness control, while the latter enables controlled friction. Efficient stiffness control can also be realized through the utilization of serial-stiffness-switch systems [38]. To achieve the effect of controlled damping one can consider implementing electromagnetic devices of the motional type [39]. Recent developments of semi-active inerters [40–42] have also enabled the real-time tuning of inertance.

3. Decentralized control design

For each subsystem $S_k(x_k)$ with associated subcontroller $C_k(u_k)$ the aim is to design control functions $u_{k,1}(t), \dots, u_{k,m_k}(t)$ that guarantee the following assumptions:

A1. The closed loop system given by Eq. (2) is asymptotically stable. This assumption establishes our primary control objective, which is to ensure the effective attenuation of free vibrations.

A2. The control functions incorporate the parameters that can be tuned to achieve a desired compromise between the performance in free vibration damping and efficiency in the energy harvesting. This assumption pertains to our secondary control objective, which is to facilitate efficient energy harvesting.

A3. The controller C_k uses only the state information of its local subsystem S_k and subsystems S_j, $j \in \mathcal{G}_k$, that are connected to S_k, i.e., it is assumed that the control functions are of the following state-feedback form:

$$u_{k,i} = u_{k,i}(x_k, \{x_j\}_{j\in\mathcal{G}_k}),\ i = 1, \dots, m_k. \tag{3}$$

This assumption defines the architecture of the decentralized state-feedback controller, considering the modular system arrangement as introduced in Section 2. The selection of state-dependence in the control function, as in Eq. (3), will subsequently enable the computation and integration of estimated interacting forces, a critical component for achieving a high level of control performance concerning the objectives outlined in A1 and A2. It is noteworthy that for the majority of modular systems, where subsystems are dynamically coupled with adjacent ones, any reconfiguration involving the addition or removal of modules does not require supplementary programming efforts when implementing the control law as defined in Eq. (3).

To design the control that satisfies assumptions A1–A3, we will first develop a representation of the interacting forces (Section 3.1). This will enable us to introduce extended state vectors and represent the dynamical Eq. (2) in the autonomous form, which is necessary to derive a stabilizing control law that satisfies assumption A1 (Section 3.2). Next, we will choose parameters that provide a balance between structural state convergence rates and amount of harvested energy as stated in assumption A2. Eventually, we will validate the proposed control law based on the decentralized controller architecture defined in assumption A3.

3.1. Dynamical model of the interaction forces

For each subsystem S_k, $k = 1, \dots, K$, we aim at characterizing the interaction forces $F_{k,j,r}$, $j \in \mathcal{G}_k$, $r = 1, \dots, r_{k,j}$, in the form of the linear differential equations that can be integrated with the dynamical Eq. (2) by extending the state vector and system matrices without violating its bilinear structuring. For that matter, we will employ dynamical autoregressive (AR) model that confirmed a high performance in reproducing the characteristics of typical polyharmonic vibrations [43]. The model will be updated periodically to capture rapid changes in the interaction forces' characteristics, which are common in modern structures that have a high level of responsiveness due to their reduced mass. For the sake of simplicity, the analysis will assume that $r_{k,j} = 1$, and will substitute $F_{k,j,r}$ with $F_{k,j}$.

It is assumed that each subcontroller C_k, $k = 1, \dots, K$, continuously collects the state information of its local subsystem x_k at a sampling period $\Delta t > 0$. Let $h_- > 0$ represent a past measurement horizon and consider a time instant $t' \in [h_-, T)$ when subcontroller C_k receives from subcontrollers C_j, $j \in \mathcal{G}_k$, the sequences of state information $x_j(t'_1), \dots, x_j(t'_p)$, where $t'_1 = t' - h_-, \dots, t'_p = t'$ and $p = h_-/\Delta t + 1$. Using this information, subcontroller C_k estimates the sequences of the interaction forces $F_{k,j}(t'_1), \dots, F_{k,j}(t'_p)$, $j \in \mathcal{G}_k$. This estimation is, for example, based on the displacements between the adjacent subsystem elements if they are interconnected with springs. The next step is to construct autoregressive (AR) models to predict the interaction forces' behaviour in a future time interval $t \in (t', t' + h_+]$, where $h_+ > 0$ is the control updating period. The evolution of $F_{k,j}$ in $t \in (t', t' + h_+]$ can be characterized by an AR model of order q:

$$F_{k,j}(t' + l\,\Delta t) = \alpha^1_{k,j}\, F_{k,j}(t' + (l-1)\,\Delta t) + \cdots + \alpha^q_{k,j}\, F_{k,j}(t' + (l-q)\,\Delta t), \quad l = 1, \dots, l_+ = h_+/\Delta t, \tag{4}$$

using previously estimated sequence $F_{k,j}(t'_1), \dots, F_{k,j}(t'_p)$ for the initial values. The weighting parameters $\alpha^1_{k,j}, \dots, \alpha^q_{k,j}$ in (4) are computed so that the AR model gives the best agreement (in some sense, such as least squares) with the samples $F_{k,j}(t'_1), \dots, F_{k,j}(t'_p)$. For a thorough study on AR model calibration methods, see [44]. To write the iterative model (4) in the form of a dynamical system, for each pair k, j we define a $q \times 1$ vector $\bar{F}_{k,j} = [\bar{F}^1_{k,j}, \dots, \bar{F}^q_{k,j}]^T$, with entries given by:

$$\bar{F}^1_{k,j}(t') = F_{k,j}(t'), \dots, \bar{F}^q_{k,j}(t') = F_{k,j}(t' + (1-q)\,\Delta t). \tag{5}$$

By introducing the matrix:

$$\bar{A}_{k,j} = \frac{1}{\Delta t} \begin{bmatrix} \alpha^1_{k,j} - 1 & \alpha^2_{k,j} & \cdots & \alpha^q_{k,j} \\ 1 & -1 & & \\ & \ddots & \ddots & \\ & & 1 & -1 \end{bmatrix} \tag{6}$$

the AR model (4) can be represented by:

$$\bar{F}_{k,j}(t' + l\,\Delta t) = \bar{F}_{k,j}(t' + (l-1)\,\Delta t) + \Delta t\, \bar{A}_{k,j}\, \bar{F}_{k,j}(t' + (l-1)\,\Delta t). \tag{7}$$

For a sufficiently small sampling period Δt, the following approximation can be used:

$$\bar{F}_{k,j}(t' + l\,\Delta t) = \bar{F}_{k,j}(t' + (l-1)\,\Delta t) + \Delta t\, \frac{\mathrm{d}\bar{F}_{k,j}}{\mathrm{d}t}. \tag{8}$$

Form (7) and (8), it follows that $\bar{F}_{k,j}$ for $t \in (t', t' + h_+]$ can be evaluated by using the linear differential equation:

$$\dot{\bar{F}}_{k,j}(t) = \bar{A}_{k,j}\, \bar{F}_{k,j}(t), \quad \bar{F}_{k,j}(t') = \bar{F}^{t'}_{k,j}, \tag{9}$$

with the initial condition $\bar{F}^{t'}_{k,j} = [F_{k,j}(t'_p), \dots, F_{k,j}(t'_{p-q+1})]^T$. For the sake of the control algorithm that will be developed in Section 3.3 it is essential to guarantee that the dynamical system describing the interaction forces is asymptotically stable. To guarantee that, each function $\bar{F}_{k,j}$ will be approximated by $\bar{x}_{k,j}$ using the exponential decay function:

$$\bar{x}_{k,j}(t) = \exp^{-\beta_{k,j} t}\, \bar{F}_{k,j}(t), \tag{10}$$

In (10), the decay parameter $\beta_{k,j}$ is computed using the spectrum of the matrix $\bar{A}_{k,j}$:

$$\beta_{k,j} = \begin{cases} 0, & \text{if } \lambda_{max}(\bar{A}_{k,j}) < 0, \\ \lambda_{max}(\bar{A}_{k,j}) + \epsilon, & \text{otherwise}, \end{cases} \tag{11}$$

In (11), $\lambda_{max}(\bar{A}_{k,j})$ stands for the largest of the real parts of the eigenvalues of $\bar{A}_{k,j}$ and $\epsilon > 0$ is some small number. From (11), it follows that $\bar{A}_{k,j} - \beta_{k,j}\mathbb{I}$ (here $\mathbb{I}$ denotes $q \times q$ identity matrix) is a Hurwitz matrix and consequently the system:

$$\dot{\bar{x}}_{k,j}(t) = (\bar{A}_{k,j} - \beta_{k,j}\mathbb{I})\, \bar{x}_{k,j}(t) \tag{12}$$

is asymptotically stable. To simplify the notation, for each $k = 1, \dots, K$, we introduce the accumulated vector $\bar{x}_k = [\{\bar{x}_{k,j}\}_{j \in \mathcal{G}_k}]^T$ and matrix $\bar{A}_k = \mathrm{diag}(\{\bar{A}_{k,j} - \beta_{k,j}\mathbb{I}\}_{j \in \mathcal{G}_k})$. Then, each subsystem S_k in $t \in (t', t' + h_+]$ is subjected to the interaction forces characterized by the dynamical equation:

$$\dot{\bar{x}}_k(t) = \bar{A}_k\, \bar{x}_k(t), \quad \bar{x}_k(t') = \bar{x}^{t'}_k, \tag{13}$$

where the initial condition is given by $\bar{x}^{t'}_k = [\{\bar{F}^{t'}_{k,j}\}_{j \in \mathcal{G}_k}]^T$. In the control algorithm (see Section 3.3), the matrix $\bar{A}_k$ in (13) will be consecutively recomputed using a predefined updating time sequence $t' = \{\tau_1, \dots, \tau_Z\}$, $\tau_1 \geq h_-$, $\tau_Z < T$, where the subsequent values are defined by the assumed control updating period, i.e., $\tau_{z+1} - \tau_z = h_+$, $z = 1, \dots, Z-1$.

3.2. Decentralized control functions

Incorporating the derived interaction forces model (13) into the structure's dynamics (2) we obtain the following autonomous linear differential equation:

$$\begin{bmatrix}\dot{x}_k(t)\\ \dot{\bar{x}}_k(t)\end{bmatrix} = \begin{bmatrix}A_k & \tilde{A}_k\\ 0 & \bar{A}_k\end{bmatrix}\begin{bmatrix}x_k(t)\\ \bar{x}_k(t)\end{bmatrix} + \sum_{i=1}^{m_k} u_{k,i}(t)\begin{bmatrix}B_{k,i} & 0\\ 0 & 0\end{bmatrix}\begin{bmatrix}x_k(t)\\ \bar{x}_k(t)\end{bmatrix},\ \begin{bmatrix}x_k(0)\\ \bar{x}_k(0)\end{bmatrix} = \begin{bmatrix}x_k^0\\ \bar{x}_k^0\end{bmatrix}. \tag{14}$$

In (14), $\tilde{A}_k$ is the matrix accommodating the interaction forces model and its composition relies on the structuring of the vectors $D_{k,j}$, $j \in \mathcal{G}_k$. For the sake of the further analysis, we introduce the extended state vector and matrices:

$$y_k(t) = \begin{bmatrix}x_k(t)\\ \bar{x}_k(t)\end{bmatrix},\ \mathcal{A}_k = \begin{bmatrix}A_k & \tilde{A}_k\\ 0 & \bar{A}_k\end{bmatrix},\ \mathcal{B}_{k,i} = \begin{bmatrix}B_{k,i} & 0\\ 0 & 0\end{bmatrix}, \tag{15}$$

and represent Eq. (14) in a compact form:

$$\dot{y}_k(t) = \mathcal{A}_k\, y_k(t) + \sum_{i=1}^{m_k} u_{k,i}(t)\,\mathcal{B}_{k,i}\, y_k(t),\ \ y_k(0) = y_k^0. \tag{16}$$

Each subsystem S_k governed by Eq. (16) will be operated with the following switching control law:

$$u_{k,i}(t) = \begin{cases} u_{min}, & y_k^T(t) P\,\mathcal{B}_{k,i}\, y_k(t) \geq 0,\\ u_{max}, & y_k^T(t) P\,\mathcal{B}_{k,i}\, y_k(t) < 0,\ \ i = 1,\dots,m_k,\end{cases} \tag{17}$$

where P is a symmetric matrix, which is computed by solving the Lyapunov equation:

$$(\mathcal{A}_k^T + \sum_{i=1}^{m_k} u_{max}\,\mathcal{B}_{k,i}^T)P + P(\mathcal{A}_k + \sum_{i=1}^{m_k} u_{max}\,\mathcal{B}_{k,i}) = -Q_k. \tag{18}$$

In (18), Q_k is a positive definite matrix and its composition will be studied in the sequel of this section. Firstly, we shall demonstrate that the control function as in (17) guarantees the asymptotic stability of the system (16) around the equilibrium point $y_k = 0$ as required in the assumption A1. For this purpose we introduce the Lyapunov function $V = V(y_k)$ given by:

$$V(y_k) = y_k^T\, P\, y_k. \tag{19}$$

Computing the time derivative of V we obtain:

$$\dot{V} = \dot{y_k}^T P y_k + y_k^T P \dot{y}_k. \tag{20}$$

The substitution of the dynamical Eq. (16) into (20) results in:

$$\dot{V} = y_k^T \mathcal{A}_k^T P y_k + y_k^T P \mathcal{A}_k y_k + \sum_{i=1}^{m_k} u_{k,i}\, y_k^T \mathcal{B}_{k,i}^T P x + \sum_{i=1}^{m_k} u_{k,i}\, y_k^T P \mathcal{B}_{k,i} y_k \tag{21}$$

which can be represented as follows:

$$\dot{V} = y_k^T(\mathcal{A}_k^T + \sum_{i=1}^{m_k} u_{max}\,\mathcal{B}_{k,i}^T)P y_k + y_k^T P(\mathcal{A}_k + \sum_{i=1}^{m_k} u_{max}\,\mathcal{B}_{k,i}) y_k + \sum_{i=1}^{m_k}(u_{k,i} - u_{max})\, y_k^T(\mathcal{B}_{k,i}^T P + P\mathcal{B}_{k,i}) y_k. \tag{22}$$

The insertion of the Lyapunov Eq. (18) and the symmetry of the matrix $P = P^T$ allows us to represent Eq. (22) in the following form:

$$\dot{V} = -y_k^T Q_k y_k + 2\sum_{i=1}^{m_k}(u_{k,i} - u_{max})\, y_k^T P \mathcal{B}_{k,i} y_k. \tag{23}$$

From $Q_k \succ 0$, it follows that the first term in (23) is strictly negative for every $y_k \neq 0$. The switching control law defined in (17) ensures that:

$$\sum_{i=1}^{m_k}(u_{k,i} - u_{max})\, y_k^T P \mathcal{B}_{k,i} y_k \leq 0. \tag{24}$$

These two upper mentioned facts lead us to the conclusion that $\dot{V} < 0$ for every y_k, and therefore the asymptotic stability of the closed-loop system (16) is guaranteed.

To define the structuring of the matrix Q_k used in the Lyapunov Eq. (18), we shall now investigate the stabilizing control function (17) in the view of the quantitative performance. Since our aim is to find a consensus between efficient free vibration damping and energy harvesting, it is convenient to analyse how the selection of Q_k can influence the rates of convergence of particular states of the vector y_k. To complete that, firstly observe that the control (17) can be perceived as the solution to the following optimization problem:

$$u_{k,i}(t) = \text{argmin}_{u\in[u_{min},u_{max}]}(u - u_{max})\, y_k^T P \mathcal{B}_{k,i} y_k,\ \ \text{for every}\, t\,. \tag{25}$$

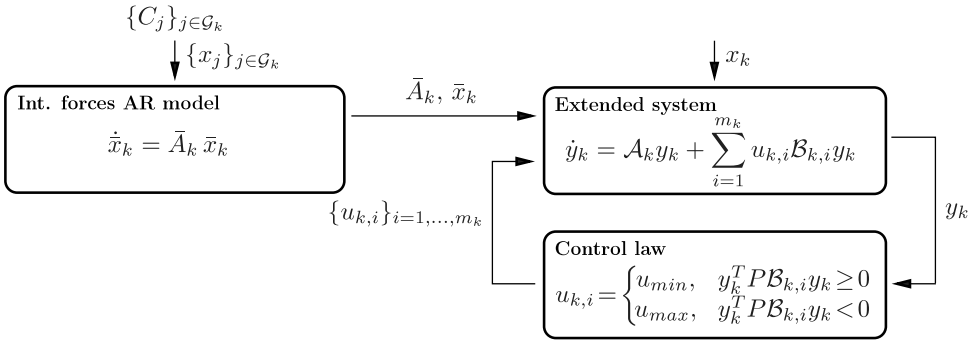

Fig. 2. Block diagram of the combined feedforward–feedback control to be operated in subcontroller C_k.

Therefore, from Eq. (23), it follows that the control (17) also fulfils the equality:

$$u_{k,i}(t) = \text{argmin}_{u\in[u_{min},u_{max}]}\{\dot{V} + y_k^T(t)Q_k y_k(t)\},\ \text{ for every } t. \tag{26}$$

Assume the diagonally structured matrix $Q_k = \text{diag}(\{q_k^l\}_{l=1,2,\dots})$ where $q_k^l = 1$ if y_k^l is a structure's state variable, and $0 < q_k^l \ll 1$, if y_k^l is a harvester's state variable. Then, Eq. (26) is of the form:

$$u_{k,i}(t) = \text{argmin}_{u\in[u_{min},u_{max}]}\{\dot{V} + q_k^1\,(y_k^1(t))^2 + q_k^2\,(y_k^2(t))^2 + \cdots\},\ \text{ for every } t. \tag{27}$$

According to Eq. (27), the control function (17) not only stabilizes the overall subsystem states, as shown in Eqs. (19)–(24), but also tends to maintain higher amplitudes of the harvester device states through the selection of the entries of Q_k. It is important to note that (27) is an instantaneous optimization problem, thus the optimal consensus of vibration suppression and energy harvesting may not be satisfied when considering a finite time horizon. However, the designed control can significantly increase the amount of harvested energy, as confirmed by the experiments presented in Section 4.5, by choosing the appropriate parameters $q_k^1, q_k^2, \dots$ that refer to assumption A2.

To demonstrate that the control function (17) meets the decentralized state-feedback structuring as defined in the assumption A3, firstly observe that the interaction forces $F_{k,j}$, $j \in \mathcal{G}_k$, can be determined using the information of the state vectors x_k and x_j, $j \in \mathcal{G}_k$. Accordingly to the assumed interaction forces model (4) each subcontroller C_k estimates the weighting parameters and composes the dynamical system (13) to perform the computation of the subsequent values of the vector $\bar{x}_k$. From the composition of the extended state vector $y_k = [x_k, \bar{x}_k]^T$ (see Eq. (15)), it follows that the control function (17) fulfils the condition $u_{k,i}(t) = u_{k,i}(x_k, \{x_j\}_{j\in\mathcal{G}_k})$.

3.3. Computational algorithm of the decentralized controller

In the following, we summarize the methodology we developed by presenting a computational algorithm to be implemented in the decentralized controller. The algorithm comprises ten major steps: Step 1 is acquiring the system matrices and control parameters. Step 2 is initializing time and control. Step 3 is verifying the terminal condition. Step 4 is identifying the time instants for updating the interaction forces and control. Steps 5 to 7 are determining the weighting parameters of the interaction forces AR model. Step 8 is solving the Lyapunov equation for updating the control law. Step 9 is computing the evolution of the interaction forces, and Step 10 is implementing the updated control decision. The block diagram of the control to be implemented in each subcontroller C_k, $k = 1, \dots, K$, is illustrated in Fig. 2.

Remarks.

R1. In Step 8, a unique solution to the Lyapunov Eq. (18) is guaranteed if the matrix $\mathcal{A}_k + \sum_{i=1}^{m_k} u_{max}\,\mathcal{B}_{k,i}$ is Hurwitz (see, for example [45]). Here, the stability of the matrix $\mathcal{A}_k$ composed as in Eq. (15) follows from the stability of the assumed interaction forces model's matrix $\bar{A}_k$ (see (13)) and the stability of the structural model matrix A_k (see Eq. (2)) which in the majority of structures is provided by the presence of the material or air damping. In the case when A_k does not fulfil the stability condition, the stability of the matrix $\mathcal{A}_k + \sum_{i=1}^{m_k} u_{max}\,\mathcal{B}_{k,i}$ can still be ensured by the contribution of its second term which is concerned with inherently dissipative semi-active devices.

R2. In Steps 6 and 7, it is assumed that the number of interaction forces acting on subsystem S_k from subsystem S_j is $r_{k,j} = 1$. In the case of $r_{k,j} > 1$, the computations are repeated for $F_{k,j,r}$, $j \in \mathcal{G}_k$, $r = 1, \dots, r_{k,j}$, and the accumulated matrix $\bar{A}_k$ is built with an appropriate size in analogy to the method described in Section 3.1.

R3. Steps 1–10 are uniform for each subcontroller C_k, $k = 1, \dots, K$, and therefore system reconfiguration or expansion only requires redefining the interconnectivity sets and relevant subsystem matrices and vectors.

Algorithm 1 Computational algorithm implemented in the decentralized controller

Step 1. Initialize the subsystem matrices and vectors:
A_k, B_k, $D_{k,j}$, $j \in \mathcal{G}_k$, $k = 1, ..., K$ (see Eq. (2)).
Build the matrices $\mathcal{B}_{k,i}$, $i = 1, ..., m_k$, $k = 1, ..., K$ (see Eq. (15)).
Select matrices Q_k, $k = 1, ..., K$ (see Section Section 3.2).
Assume the minimum and maximum admissible control values u_{min}, u_{max}.
Select control time window $[0, T]$.
Assume the measurement horizon h_- and control updating period h_+ (see Section 3.1).
Assume the set of time instants for updating the interaction forces and control:
$\tau_1, ..., \tau_Z$, $\tau_1 \geq h_-$, $\tau_Z < T$, $\tau_{z+1} - \tau_z = h_+$, $z = 1, ..., Z-1$ (see Section 3.1).
Select the sampling time Δt
and compute the number of measured state samples $p = h_-/\Delta t + 1$.
Select the order q for the AR model (see Eq. (4)).
Set the index of the updating time instants $z = 1$.

Step 2. Initialize time $t = 0$ and START control
by assuming the control functions $u_{k,i}(t) = u_{max}$, $i = 1, ..., m_k$, $k = 1, ..., K$.

Step 3. If $t < T$, then proceed to the next step.
Otherwise, STOP control.

Step 4. If $t = \tau_z$, then proceed to the next step.
Otherwise, wait.

Step 5. Each subcontroller C_k, $k = 1, ..., K$, exchanges the information
on the state samples $x_k(t'_1), ..., x_k(t'_p)$, $t'_1 = \tau_z - h_-, ..., t'_p = \tau_z$,
with subcontrollers C_j, $j \in \mathcal{G}_k$.

Step 6. Each subcontroller C_k, $k = 1, ..., K$, estimates the sequences
of the interaction forces $F_{k,j}(t'_1), ..., F_{k,j}(t'_p)$, $j \in \mathcal{G}_k$.

Step 7. Each subcontroller C_k, $k = 1, ..., K$, computes the parameters
$\alpha^1_{k,j}, ..., \alpha^q_{k,j}$, $j \in \mathcal{G}_k$, for the AR model (see Eq. (4))
and composes the accumulated matrix $\bar{A}_k$
for the dynamical system defined by Eq. (13).

Step 8. Each subcontroller C_k, $k = 1, ..., K$, builds the matrix $\mathcal{A}_k$ (see Eq. (15))
and solves the Lyapunov equation to obtain the matrix P (18).

Step 9. Each subcontroller C_k, $k = 1, ..., K$, computes the vector
$\bar{x}_k(t)$ for $t \in [\tau_z, \tau_z + h_+]$ using the dynamical equation (13).

Step 10. Each subcontroller C_k, $k = 1, ..., K$, builds the extended state vector $y_k(t)$ (see Eq. (15))
employing currently measured state $x_k(t)$ and computed state $\bar{x}_k(t)$,
and applies the control functions $u_{k,i}(t)$, $i = 1, ..., m_k$,
using the control law given by Eq. (17).
Increment the index of the updating time instants $z = z + 1$ and go to Step 3.

4. Case study

4.1. The analysed structure

The developed control will be examined using a uniquely designed suspension platform as depicted in Figs. 3 (CAD model) and 4 (real view). The structure is composed of 12 identical modules (referred to as modules no. 1–12), each involving an aluminium cantilever beam (a) and a plastic plate mounted at the beam's end (e). Every module is equipped with an electromagnetic device made of a base standing coil and a magnet attached to the bottom of the plate. Six electromagnetic devices – attached to modules no. 1–6 – will be used to mimic the operation of semi-active actuators (d) with controllable stiffness k_u and damping b_u, the remaining six devices – attached to modules no. 7–12 – will be employed as passive energy harvesters (c) of resistance R_h and inductance L_h. Each module of the total mass m is interconnected with the adjacent modules (e.g. module no. 1 is interconnected with modules no. 2 and 7) using the springs (f) of the stiffness k_s. For the beams, we assume low speed motion with the first natural mode and represent them as simple oscillators of stiffness k_b. Since the maximal deflection of the beam's end is significantly lower than the beam's length (less than 3%), we neglect the plate's rotation, and for the structural state variables, for each module, assume plate's vertical position and velocity. The structural state variables will be estimated using high-precision laser sensors (b). For the implementation of the controller, we will use a workstation (h) equipped with PCI multichannel analog I/O cards. To control the semi-active actuators,

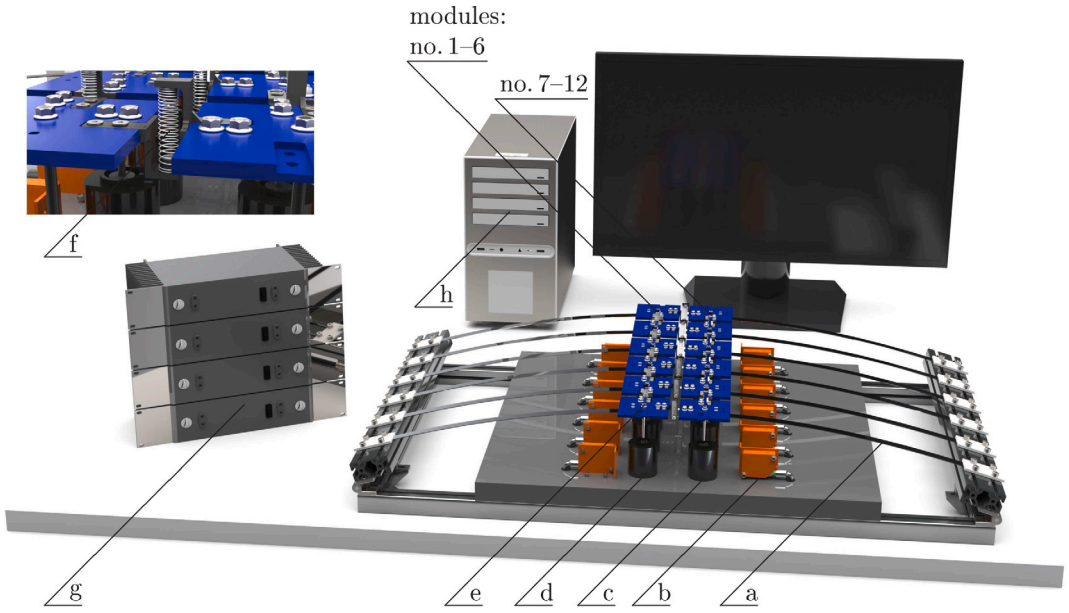

Fig. 3. CAD model of the test rig involving the modular suspension platform.

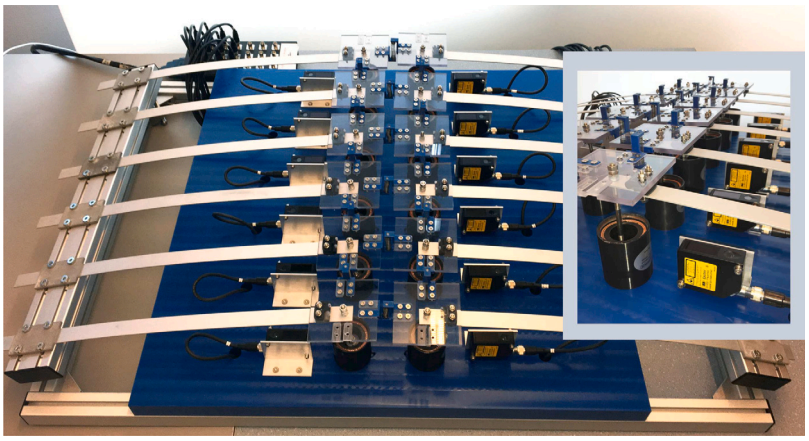

Fig. 4. Real view of the modular suspension platform.

we will employ a set of specially manufactured highly responsive power amplifiers (g). The parameters of the investigated system are listed in Table 1.

For the semi-active actuators – represented by the electromagnetic devices of modules no. 1–6 – it is assumed that the control input $u_{k,i}$ influences the stiffness $k_u(u_{k,i})$ and damping $b_u(u_{k,i})$ coefficients. Furthermore, each of these coefficients is assumed to depend linearly on the control:

$$k_u(u_{k,i}) = u_{k,i}k_u, \quad b_u(u_{k,i}) = u_{k,i}b_u. \tag{28}$$

In (28), k_u and b_u are assumed to be constant (see Table 1), and the control variable $u_{k,i}$ is switched between the values $u_{min} = 0.1$ and $u_{max} = 1$. Let us consider the module no. 1 of the subsystem S_k, where the variables $x_{k,1}$, $x_{k,2}$ and $u_{k,1}$ stand for the plate's vertical position, velocity and control input, respectively. The force produced by the semi-active actuator F_u is assumed as the sum of the elastic and damping forces:

$$F_u = -u_{k,1}k_u x_{k,1} - u_{k,1}b_u x_{k,2}. \tag{29}$$

The voltage applied from the power amplifier to the electromagnetic device is proportional to the force as in Eq. (29).

Table 1
The parameters of the modular suspension platform.

Parameter	Value
Module mass (m)	0.48 [kg]
Beam stiffness (k_b)	45 [N/m]
Spring stiffness (k_s)	22 [N/m]
Actuator stiffness coefficient (k_u)	50 [N/m]
Actuator damping coefficient (b_u)	0.5 [Ns/m]
Harvester resistance (R_h)	250 [Ω]
Harvester inductance (L_h)	0.076 [H]
Harvester mechanical–magnetic coupling constant (k_t)	14.512 [·]
Min./Max. control value (u_{min}/u_{max})	0.01/1 [·]

For the energy harvesters – represented by the electromagnetic devices of modules no. 7–12 – we will use the standard model of the coupled mechanical–magnetic system (see [29]) which constitutes that the Lorentz force on the harvester's magnet is proportional to the electric current in the coil, and the magnetic flux through the coil is composed by the self inducted flux and the flux due to the magnet motion. For the module no. 7 of the subsystem S_k assume the variables $x_{k,4}$ and $x_{k,5}$ denoting the magnet's velocity and electric current in the coil, respectively. According to the assumed mechanical–magnetic model, the Lorentz force acting on the harvester's magnet is as follows:

$$F_h = -k_t x_{k,5}. \tag{30}$$

In (29), k_t is constant obtained experimentally (see Table 1). The dynamical equation for the harvester's coil electric circuit is given by:

$$\dot{x}_{k,5} = k_t x_{k,4} - \frac{R_h}{L_h} x_{k,5}. \tag{31}$$

The complete dynamical equation for the subsystem aggregating modules no. 1 and 7 will be presented in the following section.

4.2. Subsystems selection

Since the aim is to examine how the selection of the structure's subsystems impacts on the performance of the developed decentralized control, three different architectures will be analysed. In the first case, referred to as the *decentralized variant 2* (see Fig. 5a), the suspension platform is divided into six subsystems S_1-S_6, where each collects two adjacent modules, one equipped with the semi-active actuator and the other with the energy harvester (we assume modules no. 1 and 7 for subsystem S_1, modules no. 2 and 8 for subsystem S_2, and so forth). In this arrangement, the inter-connectivity sets defined as in Eq. (1) are defined as follows:

$$\mathcal{G}_1 = \{2\},\ \mathcal{G}_k = \{k-1, k+1\}, k = 2, \dots, 5,\ \mathcal{G}_6 = \{5\}. \tag{32}$$

For subsystem $S_1(x_1)$, the state vector $x_1 = [x_{1,1}, \dots, x_{1,5}]^T$ contains respectively the position and velocity of module no. 1, the position and velocity of module no. 7 and the electric current in the circuit of the harvester of module no. 7. Subcontroller $C_1(u_1)$ associated to the subsystem $S_1(x_1)$ is operated with a single control input $u_{1,1}$. Taking into consideration the assumptions stated for the cantilever beams, semi-active actuator and energy harvester (see Eqs. (28)–(31)), and respecting the fact that the modules no. 1 and 7 are dynamically coupled by the spring of stiffness k_s, the dynamical equation for subsystem S_1 is of the following form:

$$\dot{x}_1(t) = A_1\, x_1(t) + u_{1,1}(t)\, B_{1,1}\, x_1(t) + D_{1,2,1}\, F_{1,2,1}(t) + D_{1,2,2}\, F_{1,2,2}(t),\ \ x_1(0) = x_1^0, \tag{33}$$

where the subsystem matrices are given by:

$$A_1 = \begin{bmatrix} 0 & 1 & 0 & 0 & 0 \\ -(k_b+k_s)/m & 0 & k_s/m & 0 & 0 \\ 0 & 0 & 0 & 1 & 0 \\ k_s/m & 0 & -(k_b+k_s)/m & 0 & -k_t/m \\ 0 & 0 & 0 & k_t & -R_h/L_h \end{bmatrix},\ \ B_{1,1} = \begin{bmatrix} 0 & 0 & 0 & 0 & 0 \\ -k_u/m & -b_u/m & 0 & 0 & 0 \\ 0 & 0 & 0 & 0 & 0 \\ 0 & 0 & 0 & 0 & 0 \\ 0 & 0 & 0 & 0 & 0 \end{bmatrix}. \tag{34}$$

Since the modules of the adjacent subsystems are interconnected with springs, in (33), the interaction force $F_{1,2,1}(t)$ is computed by using the relative displacement of the modules no. 1 and 2, and this information is acquired by exchanging the state information between subcontroller C_1 and C_2. Similarly, to estimate $F_{1,2,2}(t)$, subcontroller C_1 uses the relative displacement of the modules no. 7 and 8. The vectors accommodating the interaction forces in the dynamical system (33) are defined as follows $D_{1,2,1} = [0,1,0,0,0]^T$, $D_{1,2,2} = [0,0,0,1,0]^T$. The governing equations for the subsystems S_2-S_6 are built in analogy to Eq. (33) and incorporate the interaction forces established following the interconnectivity sets as defined in Eq. (32).

For the second controller's architecture, referred to as the *decentralized variant 1* (see Fig. 5b), the structure is assumed to be partitioned into subsystems S_1 and S_2, where S_1 collects the modules no. 1–3 and no. 7–9, and S_2 is composed of the modules

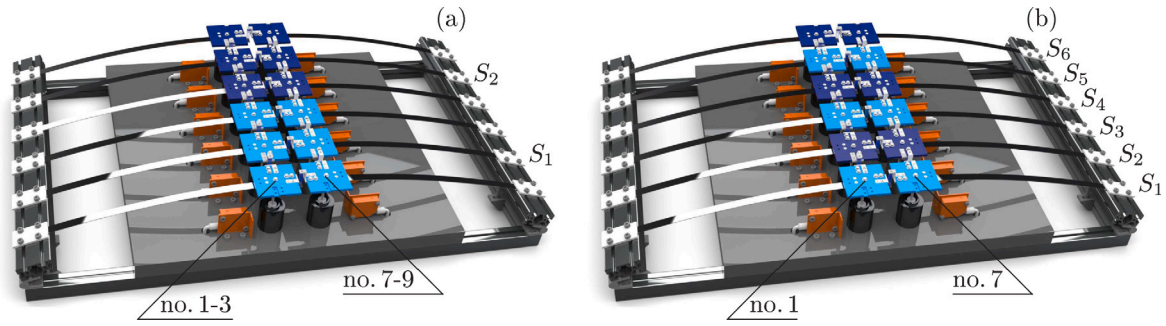

Fig. 5. Subsystems selection in the case of decentralized architectures in variant 1 (a) and 2 (b). In the case of the variant 1, the subsystem S_1 collects the modules no. 1–3 and 7–9. In the case of the variant 2, the subsystem S_1 is composed of the modules no. 1 and 7.

no. 4–6 and no. 10–12. Each subsystem relies on three control inputs and three energy harvesters. The dynamical equations and interacting forces are determined by analogy to the variant 2.

Eventually, we shall examine the developed method for the *centralized* controller architecture, where the global system S contains all modules no. 1–12 and is operated with a single computing unit C that controls six inputs. In this case, the interconnectivity set is empty, and consequently the interaction forces vanish.

4.3. Selection of the control algorithm parameters

The experiments are conducted in the MATLAB environment. The main code is divided into separate sections, simulating the collaboration of the subcontrollers in accordance with the assumed architectures (see Section 4.2). For each subcontroller, Algorithm 1 is implemented using the following settings. The entries in the matrices Q_k, $k = 1, \dots, K$, corresponding to the states of the harvesters, are assumed to be equal to 0.00001. The control time window and the measurement horizon are assumed to be $T = 20[s]$ and $h_- = 0.02[s]$, respectively. The control algorithm's sampling time is set to $\Delta t = 0.002[s]$, resulting in $p = 11$ state samples being exchanged by the interconnected subcontrollers when predicting the evolution of the interaction forces. To reduce the measurement noise generated by the laser sensors, the sampling time on the PCI I/O devices is set to $0.0005[s]$, and four consecutive values are averaged to obtain the actual state value used in the control algorithm, which operates with the sampling time $\Delta t = 0.002[s]$. During the time interval $[0.02, 20][s]$, the following set of time instants for updating the interaction forces and control are assumed: $\tau_1 = 0.02[s], \dots, \tau_Z = 19.92[s]$, with a constant update interval of $h_+ = 0.1[s]$. The order of the AR model of the interaction forces is assumed to be $q = 4$, and this selection is made by trial and error, using the criterion of compromising the accuracy of the evolution of the interaction forces with the computational time, which is limited to 10% of the update period h_+. To estimate the AR model parameters (see Step 7), the MATLAB "arburg" function is used. The solution to the Lyapunov equation (see Step 8) is obtained using the MATLAB "lyap" function. The integration of the interaction forces' dynamic equations (see Step 9) is performed using the Runge–Kutta fourth-order scheme with a time step equal to the algorithm's sampling time Δt. For each of the considered cases, the average total time required to compute the updated control (Step 3–Step 10) was below 0.016 [s] (the procedure was run using a workstation with an Intel Xeon, 3.00 GHz, 16 GB, that operated on the Linux platform).

4.4. Comparative controls

To assess the performance of the developed control, it will be compared with an alternative decentralized control method, referred to as the *heuristic control*, and the *passive damping* strategy.

The heuristic control is based on the principle of isolating each subsystem, which for the system as in Eq. (2) is equivalent to assuming that interaction forces are negligible, i.e., $F_{k,j} = 0$, $j \in \mathcal{G}_k$. The control law is derived by maximizing the rate of energy dissipation in each subsystem instantaneously (see [14]). Experiments have shown (see [46]) that this method is highly effective in stabilizing the free vibrations of a structure equipped with semi-active elastomer-based blocks that generate controlled forces as defined in Eq. (29). Additionally, the heuristic control can be implemented in the control architectures outlined in Section 4.2. The main difference between the heuristic and developed methods lies in the amount of state information used in the feedback loop, with the heuristic control excluding the state of adjacent subsystems. To derive the control function for the heuristic method and ensure it is consistent with the assumptions made for the developed control, we define the energy-related function for each subsystem C_k, $k = 1, \dots, K$:

$$E_k(t) = x_k^T(t)\, \bar{Q}_k\, x_k(t), \tag{35}$$

where $\bar{Q}_k$ is a submatrix of Q_k (see Eq. (18)) that collects only those entries of Q_k that correspond to the structure's state vector x_k. The heuristic control functions $u_{k,i}^h(t)$, $i = 1, \dots, m_k$, that guarantee the best instantaneous dissipation of the energy E_k are given as the solution to the following optimization problem:

$$u_{k,i}^h(t) = \text{argmin}_{u_{k,i} \in [u_{min}, u_{max}]}\, \dot{E}_k(t), \;\; i = 1, \dots, m_k. \tag{36}$$

Table 2
Comparison of the mechanical energy integral J_m, total harvested energy $E_h(T)$ and efficiency parameter $E_h(T)/J_m$ for the Case A. For each control method, the values are normalized to the passive damping strategy.

	Passive	Designed control			Heuristic control		
		Centr.	Decentr. v1	Decentr. v2	Centr.	Decentr. v1	Decentr. v2
J_m	1.0000	0.4146	0.4282	0.4309	0.4173	0.4634	0.5962
$E_h(T)$	1.0000	0.5516	0.5693	0.5740	0.5513	0.5811	0.7390
$E_h(T)/J_m$	1.0000	1.3304	1.3295	1.3321	1.3211	1.2540	1.2395

The time derivative of the energy function can be computed as follows:

$$\dot{E}_k = \dot{x}_k^T \bar{Q}_k x_k + x_k^T \bar{Q}_k \dot{x}_k. \tag{37}$$

From the symmetry of the matrix $\bar{Q}_k$ and the dynamical Eq. (2), it follows that:

$$u_{k,i}^h(t) = \begin{cases} u_{min}, & x_k^T(t)\,\bar{Q}_k B_{k,i}\, x_k(t) \geq 0, \\ u_{max}, & x_k^T(t)\,\bar{Q}_k B_{k,i}\, x_k(t) < 0, \ i = 1, \dots, m_k. \end{cases} \tag{38}$$

The reader can verify that for Hurwitz matrix A_k the control (38) guarantees $\dot{E}_k < 0$ for $x_k \neq 0$, and thus ensures the asymptotic stability of the closed-loop system given by Eq. (2) when $F_{k,j} = 0$, $j \in \mathcal{G}_k$.

For the passive damping strategy we assume constant control functions $u_{k,i}^p(t)$, $i = 1, \dots, m_k$, where each semi-active device operates at the maximal admissible value, i.e., $u_{k,i}^p(t) = u_{max}$, $i = 1, \dots, m_k$. In the vast majority of the semi-actively controlled structures, this strategy is equivalent to the optimal passive damping (see, for example [47]).

4.5. Results and discussion

The present study evaluates the efficacy of the developed method for the analysis of free vibration, while considering two different initial condition scenarios. In the first scenario, referred to as Case A, the initial configuration involves the placement of module no. 1 at a displacement of 0.02 [m], whereas the remaining modules are set to their initial position of zero displacement. The second scenario, referred to as Case B, focuses on validating the higher vibration mode of the system. This is accomplished by imposing initial deflections of 0.01, 0.02, 0.01 and 0.02 [m] for modules no. 1, 3, 4 and 6, respectively.

In order to assess the efficacy of stabilizing control performance, we will analyse a measure defined as the time integral of the mechanical energy over the control period T:

$$J_m = \int_0^T E_m(t)\,\mathrm{d}t. \tag{39}$$

In (39), $E_m(t)$ represents the mechanical energy of the entire structure, calculated as the sum of potential and kinetic energies for all 12 modules and interconnecting springs, without regard to subsystem selection. In addition, we will evaluate the total amount of harvested electrical energy, which is given by:

$$E_h(t) = \int_0^t P_m(t)\,\mathrm{d}t, \tag{40}$$

where $P_m(t)$ represents the sum of the electrical power generated by the energy harvesting devices of modules no. 7 to 12. The effectiveness of energy harvesting will be determined by comparing the total amount of harvested electrical energy to the total mechanical energy, calculated as the ratio $E_h(T)/J_m$. In order to conduct a rigorous examination as expounded in Sections 4.5.1 and 4.5.2, we will determine each of the aforementioned metrics by computing the mean value resulting from three successive experimental trials.

4.5.1. Case A

We commence our analysis by comparing the evolution of the mechanical energy $E_m(t)$ obtained through the passive damping strategy and the designed and heuristic control techniques, while considering the subsystems selection of the decentralized variant 2. This comparison is depicted in Fig. 6a and confirms that the designed control exhibits a high stabilizing performance. Specifically, the results indicate that after the first three seconds of the experiment the designed method resulted in mechanical energy that was 12.9% and 68.2% lower than that obtained with the heuristic control and passive strategy, respectively. The effectiveness of the designed control in stabilizing the system can also be assessed through the analysis of the deflection of module no. 1, as illustrated in Fig. 7a. The deflection trajectory resulting from the designed control demonstrated a decrease in peak amplitudes at approximately $t = 0.2$ [s] and $t = 0.4$ [s] by 9.5% and 19.4%, respectively, when compared to the heuristic control. When compared to the passive damping strategy, these reductions were 19.9% and 42.4%. The high stabilizing performance of the developed control is further confirmed by analysing the frequency responses of the deflection of module no. 1 (see Fig. 9a). The peak amplitude of this characteristic at approximately 2.5 [Hz] was reduced by 46.0% and 17.7% when compared to passive damping and heuristic control, respectively. Additionally, for both the designed and heuristic control, a slight shift of the peak amplitudes towards lower frequencies is observed, resulting from temporary drops in stiffness when applying the assumed switched control laws (see Eqs. (17) and (38)).

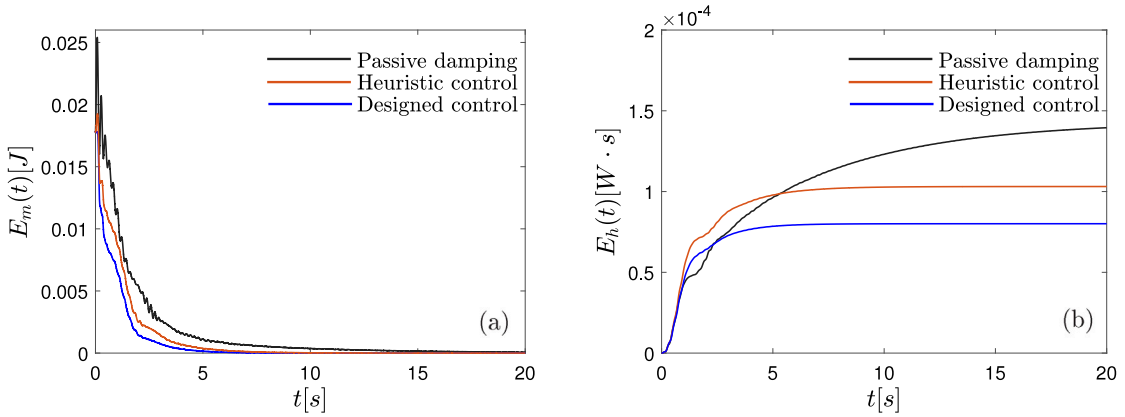

Fig. 6. The evolution of the mechanical energy E_m (a) and harvested electrical energy E_h (b) for the passive strategy, developed control and heuristic control in Case A assuming the architecture of decentralized variant 2.

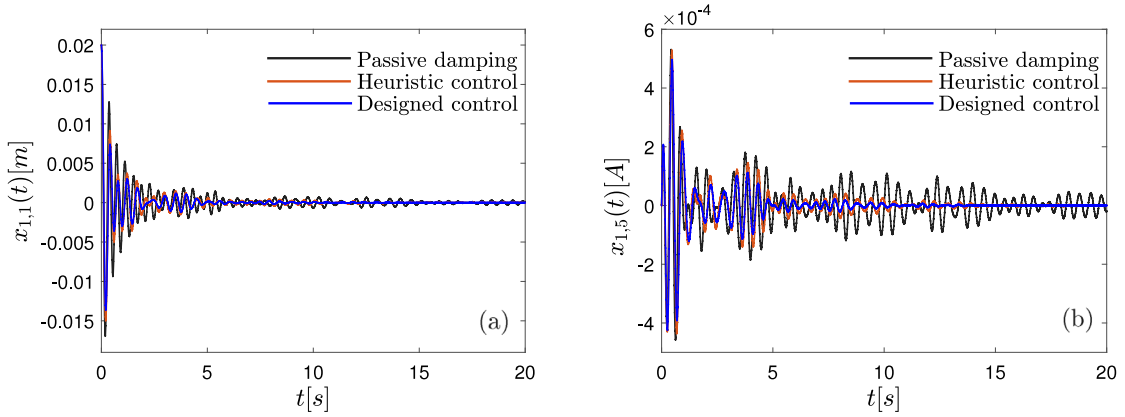

Fig. 7. The trajectories of the deflection of module no. 1 (a) and electric current in module no. 7 for the passive strategy, developed control and heuristic control in Case A assuming the architecture of decentralized variant 2.

The examination of the integral of mechanical energy J_m, as presented in Table 2, evidences that the developed control resulted in a substantial 38.3% increase in overall stabilizing performance for the decentralized variant 2 as compared to the heuristic control. In comparison to the passive method, this improvement was 132.1%. The obtained values of the integral of mechanical energy has also revealed that the decentralization of controller architecture has marginal impact on the stabilizing performance of the developed control. Specifically, when compared to the centralized architecture, the decentralized variants 1 and 2 resulted in an increase of 3.2% and 3.9% in the integral energy measure, respectively. In contrast, the heuristic control approach exhibited a considerably larger increase, 11.0% and 42.8% for the respective decentralized architectures.

Our subsequent aim is to validate the efficacy of the proposed control methodology for electrical energy harvesting. Considering that the designed control achieved superior stabilizing performance, leading to reduced vibration amplitudes and, consequently, diminished electric current in the harvesting devices (as illustrated in Fig. 7a), it is anticipated that this control approach will also result in the least amount of accumulated electrical energy. This can be confirmed by analysing the curves that represent the electrical energy $E_h(t)$ (depicted in Fig. 6b) acquired by all six harvesting devices while assuming the subsystem selection of the decentralized variant 2. Although we can identify time intervals when the developed control produces rapid increases in the electrical energy, overall, for the given control time, the increment of this energy was slower than in the remaining cases. In terms of the total harvested energy $E_h(T)$, the developed control exhibited inferior performance by 28.7% and 74.2% compared to the heuristic and passive methods, respectively. However, considering the relative efficiency of energy harvesting, as measured by the fraction $E_h(T)/J_m$ (see Table 2), the developed control outperforms the heuristic method for all controller architectures. In particular, for the decentralized variant 2, the designed control resulted in a 7.4% increase in the relative efficiency of energy harvesting. It is noteworthy that the change in controller architecture does not significantly impact the value of $E_h(T)/J_m$ when implementing the designed control. In contrast, for the heuristic control, decentralization resulted in a drop in the aforementioned value by 5.1% and 6.2% for decentralized variant 1 and 2, respectively.

Fig. 8 presents a comparison of the switching patterns obtained from the implementation of the developed control law (see (17)) across the assumed architectures for the module no. 1. It is noteworthy that despite significant differences in the capacity of state

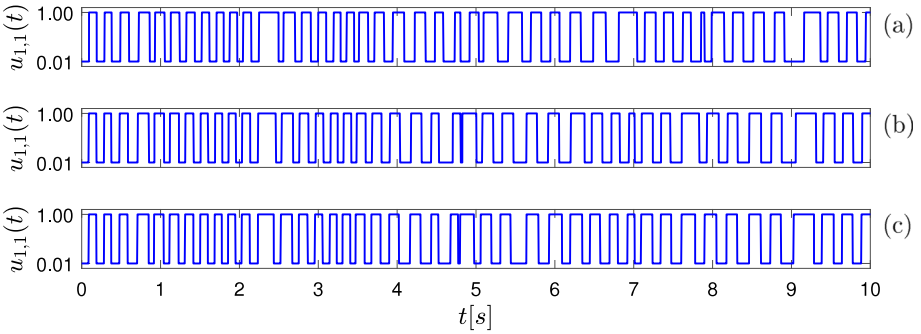

Fig. 8. The control functions of module no. 1 under the developed control for Case A, considering three different architectures: centralized (a), decentralized variant 1 (b), and decentralized variant 2 (c).

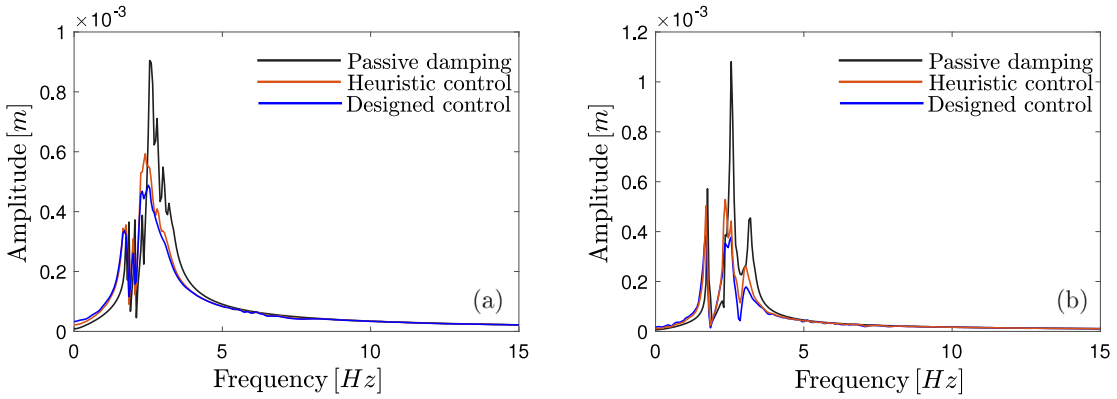

Fig. 9. The amplitude–frequency characteristics of the deflection of module no. 1 for the passive strategy, developed control, and heuristic control in Case A (a) and B (b), considering the architecture of the decentralized variant 2.

Table 3
Comparison of the mechanical energy integral J_m, total harvested energy $E_h(T)$ and efficiency parameter $E_h(T)/J_m$ for the Case B. For each control method, the values are normalized to the passive damping strategy.

	Passive	Designed control			Heuristic control		
		Centr.	Decentr. v1	Decentr. v2	Centr.	Decentr. v1	Decentr. v2
J_m	1.0000	0.4298	0.4472	0.4548	0.4363	0.5419	0.6126
$E_h(T)$	1.0000	0.5566	0.5798	0.5901	0.5368	0.6464	0.7275
$E_h(T)/J_m$	1.0000	1.2950	1.2965	1.2975	1.2303	1.1928	1.1876

information utilized by the control functions, the overall switching pattern is similar in each case. Specifically, during the first two seconds of the experiments, when the vibration amplitudes sustain at high levels, any deviation between the analysed switching trajectories is negligible. During the remaining time, a gradual divergence of the switching points of the centralized and decentralized controls is observed, whereas the controls of the decentralized architectures exhibit close alignment. These observations confirm that the inclusion of interacting forces that replicate the structural coupling between subsystems facilitates the reduction of the effect of decentralization degree on the control characteristics and its overall performance.

4.5.2. Case B

The following experiments were carried out to examine the effectiveness of the proposed approach for higher vibration mode. Specifically, the investigation aimed to assess the impact of higher frequency vibrations on the accuracy of predicting the interaction forces using the assumed autoregressive model and its consequent effect on the overall control performance. It should be emphasized that the parameters of the autoregressive model employed in this study are identical to those utilized in Case A (see Section 4.3).

Upon analysing the mechanical energy curves demonstrated in Fig. 10a, it can be observed that the overall stabilizing performance of the designed decentralized controller is maintained in this case. Furthermore, similar to Case A, the values of the integral of mechanical energy resulting from the centralized and decentralized architectures nearly coincide for the developed control, with a marginal increase of 4.0% and 5.8% as a result of decentralization into the architectures of variant 1 and 2, respectively (see Table 3). It is noteworthy that the heuristic strategy resulted in a 24.0% increase in the integral of mechanical

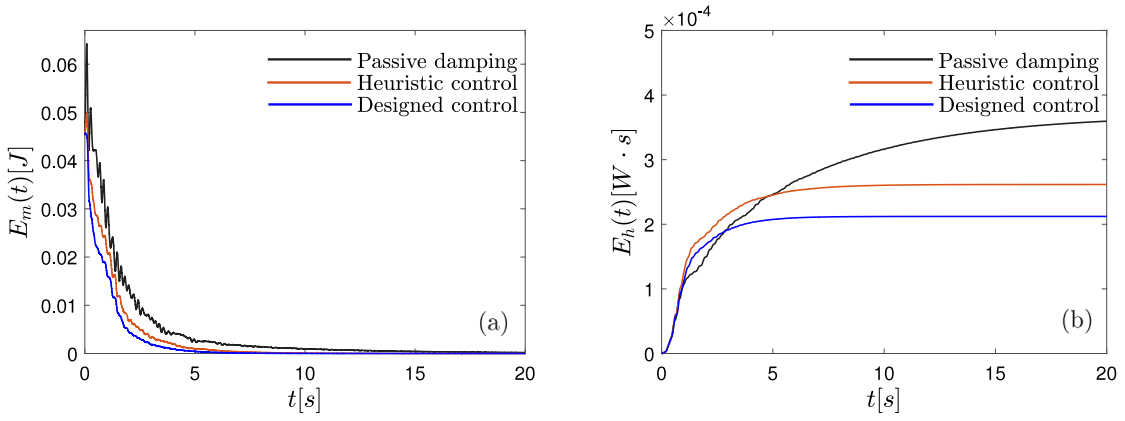

Fig. 10. The evolution of the mechanical energy E_m (a) and harvested electrical energy E_h (b) for the passive strategy, developed control and heuristic control in Case B assuming the architecture of decentralized variant 2.

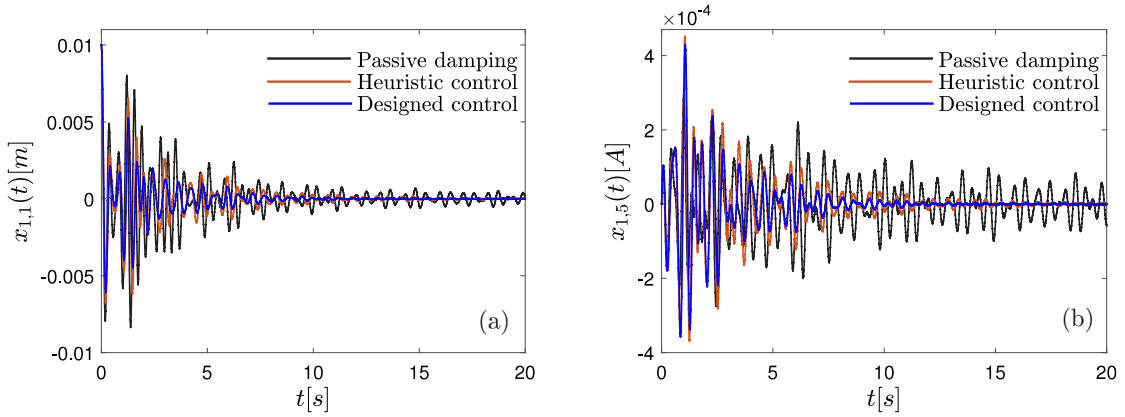

Fig. 11. The trajectories of the deflection of module no. 1 (a) and electric current in module no. 7 for the passive strategy, developed control and heuristic control in Case B assuming the architecture of decentralized variant 2.

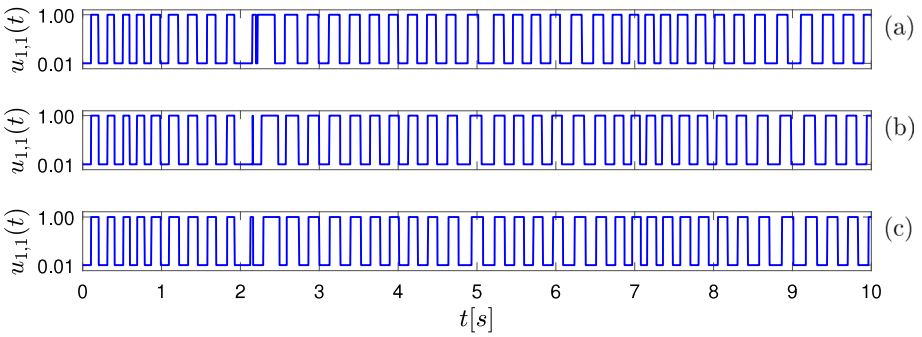

Fig. 12. The control functions of module no. 1 under the developed control for Case B, considering three different architectures: centralized (a), decentralized variant 1 (b), and decentralized variant 2 (c).

energy in variant 1 due to decentralization, which is 81.8% higher than that observed in Case A. The efficacy of the designed control in stabilizing the system under higher vibration frequencies is also supported by the deflection characteristics of module no. 1 (see Fig. 11a). A reduction in peak amplitudes by 10.6% and 19.8% is observed at approximately $t = 0.2$ [s] and $t = 1.2$ [s], respectively, when compared to the heuristic control. Moreover, these reductions were more significant when compared to the passive damping strategy, with reductions of 23.6% and 34.5% observed at the same time instants, respectively. Examining the frequency responses of the deflection of module no. 1, as depicted in Fig. 9b, we observe that the designed control leads to a decrease in the dominant peak at approximately 2.5 [Hz] by 65.1% and 28.5% when compared to passive damping and heuristic control,

Table 4
Comparison of the mechanical energy integral J_m, total harvested energy $E_h(T)$ and efficiency parameter $E_h(T)/J_m$ for the assumed measurement system failure. For each control method, the values are normalized to the passive damping strategy.

	Passive	Designed control			Heuristic control		
		Centr.	Decentr. v1	Decentr. v2	Centr.	Decentr. v1	Decentr. v2
J_m	1.0000	0.5716	0.5879	0.5390	0.6391	0.6508	0.6135
$E_h(T)$	1.0000	0.7273	0.7486	0.7236	0.8056	0.8168	0.7821
$E_h(T)/J_m$	1.0000	1.2724	1.2733	1.3425	1.2605	1.2551	1.2748

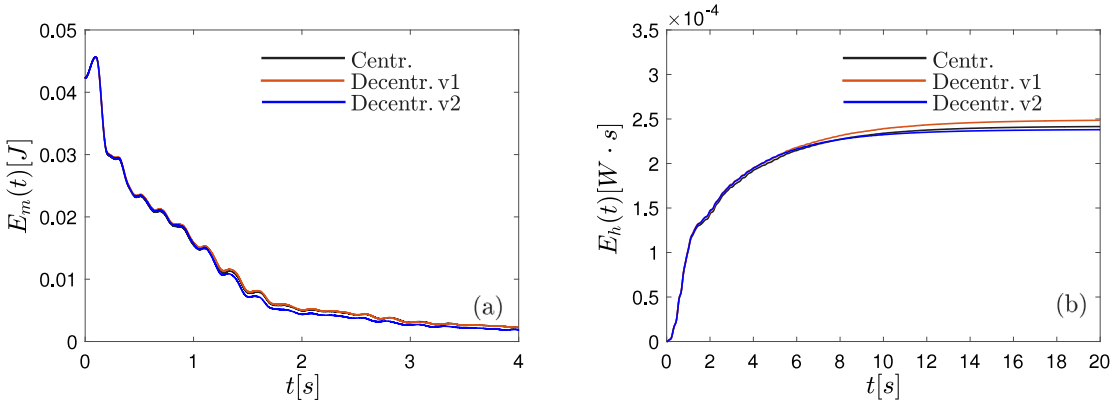

Fig. 13. The evolution of the mechanical energy E_m (a) and harvested electrical energy E_h (b) for the developed control under various controller architectures and measurement system failure.

respectively. Furthermore, the reductions of the two remaining peaks at approximately 1.7 [Hz] and 3.1 [Hz] were 32.6% and 60.8%, respectively, when compared to the damping strategy. Compared to the heuristic control, these reductions were 23.4% and 31.6%, respectively. As in the previous case, due to the temporary reduction in stiffness in the control devices, both the developed and heuristic controls exhibited a minor shift in the peak amplitudes towards lower frequencies.

Analysing the trajectories of the harvested energy (Fig. 10b) and electric current (Fig. 11b) it can be concluded that the higher vibration mode does not exert a significant influence on the efficacy of the developed methodology in terms of electric energy storage. Similar to Case A, the significant reduction in vibration amplitudes resulted in a substantial decrease in the quantity of harvested energy when compared to competitive control strategies. However, as evidenced by the results presented in Table 3, the developed control still exhibits the highest relative efficiency of energy harvesting, as quantified by the ratio of total harvested energy $E_h(T)$ to the integral of mechanical energy J_m. Specifically, the developed control outperforms the heuristic method by 8.7% and 9.2% for the decentralized variant 1 and 2, respectively. Analogous to Case A, the alteration of controller architecture has a negligible effect on the relative efficiency of energy harvesting when employing the developed control.

With regard to the controls obtained for module no. 1 (see Fig. 12), it can be observed that the switching patterns resulting from the implementation of the decentralized architectures exhibit a slightly larger deviation from the centralized architecture compared to Case A, which can be detected after two seconds of the experiments. However, the coincidence between the control function of decentralized variant 1 and 2 remains intact.

4.6. Fault tolerance analysis

The final set of experiments was conducted to examine the designed method in the context of a potential control system failure. In particular, our aim is to investigate whether the decentralization of the controller can mitigate the impact of local sensor failures, ensuring both global stabilization and sustained energy harvesting performance. For that purpose, we considered the three previously examined controller architectures and assumed initial deflections of 0.02, 0.01, 0.01 and 0.02 [m] for modules no. 1, 2, 4 and 6, respectively. Sensor failures are simulated according to the following scenario. For $t < 1$ [s], all sensors transmit accurate measurements. Subsequently, at $t = 1$ [s], the sensor of module no. 2 begins malfunctioning, sending the controller values that are equal to zero for both displacement and velocity. Subsequently, analogous malfunctioning is applied to the sensors of module no. 4 and 6, starting from $t = 2$ [s] and $t = 3$ [s], respectively. The experiment is terminated at $T = 20$ [s]. For comparison, the same scenarios were repeated with the heuristic control and passive damping strategy.

Analysing the characteristics of the mechanical energy J_m (see Fig. 13a), it is evident that in the case of proper functioning of the measurement system (i.e., for $t < 1$ [s]), the stabilizing performance of the designed control remains comparable across different controller architectures, confirming the previous results. The malfunctioning of the sensor attached to module no. 2, starting at $t = 1$ [s], results in a slow divergence of the energy curves. Specifically, the decentralized variant 2, which divides

the global system into six subsystems (see Fig. 5b), exhibits superior fault tolerance among the considered architectures. The overall stabilizing performance of this controller is further confirmed by the total energy measure J_m, which accounts for the malfunctioning of three sensors. It indicates a reduction of 6.8% and 8.4% compared to the centralized and decentralized variant 1, respectively (see Table 4). The slightly lower robustness of the decentralized variant 1 (see Fig. 5a) is concerned with relatively low level of decentralization in this architecture, where two malfunctioning sensors are included in a single subsystem S_2. A similar observation was made for the heuristic control, with a 4.1% and 5.8% reduction in the integral of the mechanical energy for decentralized variant 2 compared to the centralized and decentralized variant 1, respectively. Under the assumed faulty conditions, controller decentralization also allowed for substantial efficiency in electric energy harvesting (see Fig. 13a). Regarding the efficiency parameter $E_h(T)/J_m$, decentralized variant 2 outperforms the centralized and decentralized variant 1 by 5.5% and 5.4%, respectively. Analysing the overall performance of the developed control (see Table 4), it can be concluded that a faulty measurement system can significantly impact the efficiency in both stabilization and energy harvesting. This is clearly reflected in a decrease in improvement compared to the passive damping strategy. Nevertheless, the superiority of the proposed method over the heuristic control remains consistent, irrespective of the controller architecture.

5. Conclusions

A decentralized method for semi-active control has been proposed for the purpose of mitigating structural vibrations and harvesting energy. The method involves communication between neighbouring subcontrollers and periodic updates of the state-feedback functions which incorporate a model characterizing the interaction forces between the subsystems of the structure. The developed method is applicable to a broad class of bilinear systems and can be implemented in various types of structures where modularity is an essential characteristic. The proposed control has been evaluated through experimentation on a modular suspension platform, which was equipped with electromagnetic devices that functioned as both semi-active actuators and energy harvesters. The efficacy of the decentralized controller has been investigated in the context of free vibration scenarios and compared against a heuristic method that relies on the concept of isolated subsystems. The control developed has demonstrated a significant improvement in terms of vibration mitigation for each scenario, leading to a reduction up to 28.7% in the assumed measure of mechanical energy. In comparison to a standard passive damping approach, the proposed control technique achieved a reduction in mechanical energy with a magnitude of 74.2%. Notably, the parametrization of the suggested control law facilitated the identification of an optimal trade-off between state convergence and energy harvesting. As a result, the relative efficiency of energy harvesting demonstrated an average enhancement of 6.2% and 31.3% when compared to the heuristic and passive damping methods, respectively. An important finding of this investigation is that the performance of the developed control is only minimally affected by alterations in the controller's architecture, in contrast to the heuristic approach. Moreover, the proposed decentralized controller demonstrated robustness in a faulty measurement scenario, delivering both vibration suppression and energy harvesting. Specifically, in the case of the most decentralized architecture, the reduction in mechanical energy was 46.1% and 12.2% when compared to the passive and heuristic control, respectively. The obtained results reinforce the idea that the effectiveness of decentralized control relies on the subcontrollers' ability to communicate and estimate interactions between subsystems. Moreover, the relatively low computational cost required to implement the proposed control algorithm in decentralized architectures suggests its suitability for large-scale structures.

CRediT authorship contribution statement

Dominik Pisarski: Conceptualization, Data curation, Formal analysis, Funding acquisition, Investigation, Methodology, Project administration, Resources, Software, Validation, Visualization, Writing – original draft, Writing – review & editing. **Łukasz Jankowski:** Conceptualization, Funding acquisition, Investigation, Resources, Writing – review & editing.

Declaration of competing interest

The authors declare that they have no known competing financial interests or personal relationships that could have appeared to influence the work reported in this paper.

Data availability

Data will be made available on request.

Acknowledgements

This research has been supported by the National Science Centre, Poland under grant agreements 2020/39/B/ST8/02615 and 2017/26/D/ST8/00883.

References

[1] M. Zawidzki, Ł. Jankowski, Multiobjective optimization of modular structures: Weight versus geometric versatility in a Truss-Z system, Comput.-Aided Civ. Infrastruct. Eng. 34 (11) (2019) 1026–1040, http://dx.doi.org/10.1111/mice.12478.

[2] M.U. Demir, C. Yilmaz, A three-axis modular horizontal vibration isolation system with adjustable stiffness: Design, analysis and experimental validation, J. Sound Vib. 541 (2022) 117351, http://dx.doi.org/10.1016/j.jsv.2022.117351.

[3] X. Liu, G. Cai, K. Wang, Synthesizing and reconfiguring metastable modular metamaterials for adaptive wave propagation control, J. Sound Vib. 468 (2020) 115114, http://dx.doi.org/10.1016/j.jsv.2019.115114.

[4] L. Bakule, Decentralized control: An overview, Annu. Rev. Control 32 (1) (2008) 87–98, http://dx.doi.org/10.1016/j.arcontrol.2008.03.004.

[5] L. Bakule, M. Papik, B. Rehak, Decentralized stabilization of large-scale civil structures, Vol. 47, (3) 2014, pp. 10427–10432, http://dx.doi.org/10.3182/20140824-6-ZA-1003.00692.

[6] Y. Lei, D.T. Wu, Y. Lin, A decentralized control algorithm for large-scale building structures, Comput.-Aided Civ. Infrastruct. Eng. 27 (1) (2012) 2–13, http://dx.doi.org/10.1111/j.1467-8667.2010.00707.x.

[7] Z.J. Yang, Y. Fukushima, P. Qin, Decentralized adaptive robust control of robot manipulators using disturbance observers, IEEE Trans. Control Syst. Technol. 20 (5) (2012) 1357–1365, http://dx.doi.org/10.1109/TCST.2011.2164076.

[8] Y. Cha, A.K. Agraval, Decentralized output feedback polynomial control of seismically excited structures using genetic algorithm, Struct. Control Health Monit. 20 (2013) 241–258, http://dx.doi.org/10.1002/stc.486.

[9] S. Cinquemani, F. Braghin, Decentralized active vibration control in cruise ships funnels, Ocean Eng. 140 (2017) 361–368, http://dx.doi.org/10.1016/j.oceaneng.2017.06.008.

[10] S. Cinquemani, F. Resta, Decentralized control of vibration with active smart dampers, in: A. Erturk (Ed.), Active and Passive Smart Structures and Integrated Systems XII, Vol. 10595, SPIE, International Society for Optics and Photonics, 2018, p. 105953A, http://dx.doi.org/10.1117/12.2292644.

[11] A. Mroz, A. Orłowska, J. Holnicki-Szulc, Semi-active damping of vibrations. Prestress accumulation-release strategy development, Shock Vib. 17 (2) (2010) 123–136, http://dx.doi.org/10.3233/SAV-2009-0502.

[12] B. Popławski, G. Mikułowski, A. Mróz, Ł. Jankowski, Decentralized semi-active damping of free structural vibrations by means of structural nodes with an on/off ability to transmit moments, Mech. Syst. Signal Process. 100 (2018) 926–939, http://dx.doi.org/10.1016/j.ymssp.2017.08.012.

[13] D. Pisarski, T. Szmidt, R. Konowrocki, Decentralized semi-active structural vibration control based on optimal system modelling, Struct. Control Health Monit. 27 (11) (2020) e2624, http://dx.doi.org/10.1002/stc.2624.

[14] D. Pisarski, Decentralized stabilization of semi-active vibrating structures, Mech. Syst. Signal Process. 100 (2018) 694–705, http://dx.doi.org/10.1016/j.ymssp.2017.08.003.

[15] F. Palacios-Quiñonero, J.M. Rossell, H.R. Karimi, Semi-decentralized strategies in structural vibration control, Model. Identif. Control 32 (2) (2011) 57–77, http://dx.doi.org/10.4173/mic.2011.2.2.

[16] D.D. Šiljak, Decentralized Control of Complex Systems, Academic Press, New York, 1991.

[17] L. Bakule, F. Paulet-Crainiceanu, J. Rodellar, J.M. Rossell, Overlapping reliable control for a cable-stayed bridge benchmark, IEEE Trans. Control Syst. Technol. 13 (4) (2005) 663–669, http://dx.doi.org/10.1109/TCST.2004.841678.

[18] R.D. Verdoljak, L.E. Linderman, Sparse feedback structures for control of civil systems, Struct. Control Health Monit. 23 (11) (2016) 1334–1349, http://dx.doi.org/10.1002/stc.1847.

[19] D. Pisarski, Distributed control design for structures subjected to traveling loads, Math. Probl. Eng. 2015 (2015) 1–12, http://dx.doi.org/10.1155/2015/206870.

[20] D. Pisarski, A. Myśliński, Suboptimal distributed state-feedback control of semi-active vibrating systems, J. Sound Vib. 443 (2019) 637–651, http://dx.doi.org/10.1016/j.jsv.2018.12.009.

[21] O. Abdeljaber, O. Avci, D.J. Inman, Active vibration control of flexible cantilever plates using piezoelectric materials and artificial neural networks, J. Sound Vib. 363 (2016) 33–53, http://dx.doi.org/10.1016/j.jsv.2015.10.029.

[22] Z. Wang, F. Ubertini, S. Laflamme, Ensemble of long short-term memory recurrent neural network for semi-active control of tuned liquid wall damper, Eng. Struct. 270 (2022) 114771, http://dx.doi.org/10.1016/j.engstruct.2022.114771.

[23] A. Bathaei, S.M. Zahrai, Improving semi-active vibration control of an 11-story structure with non-linear behavior and floating fuzzy logic algorithm, Structures 39 (2022) 132–146, http://dx.doi.org/10.1016/j.istruc.2022.03.022.

[24] D. Leng, Z. Zhu, G. Liu, Y. Li, Neuro fuzzy logic control of magnetorheological elastomer isolation system for vibration mitigation of offshore jacket platforms, Ocean Eng. 253 (2022) 111293, http://dx.doi.org/10.1016/j.oceaneng.2022.111293.

[25] S. Nagendra, N. Podila, R. Ugarakhod, K. George, Comparison of reinforcement learning algorithms applied to the cart-pole problem, in: 2017 International Conference on Advances in Computing, Communications and Informatics, 2017, pp. 26–32.

[26] A. Khalatbarisoltani, M. Soleymani, M. Khodadadi, Online control of an active seismic system via reinforcement learning, Struct. Control Health Monit. 26 (3) (2019) e2298.

[27] C. Dengler, B. Lohmann, Actor-critic reinforcement learning for the feedback control of a swinging chain, IFAC Pap. 51 (2018) 378–383.

[28] D. Pisarski, Ł. Jankowski, Reinforcement learning-based control to suppress the transient vibration of semi-active structures subjected to unknown harmonic excitation, Comput.-Aided Civ. Infrastruct. Eng. 38 (12) (2023) 1605–1621, http://dx.doi.org/10.1111/mice.12920.

[29] R.A. Rojas, A. Carcaterra, An approach to optimal semi-active control of vibration energy harvesting based on MEMS, Mech. Syst. Signal Process. 107 (2018) 291–316, http://dx.doi.org/10.1016/j.ymssp.2017.11.005.

[30] G. Pepe, A. Carcaterra, VFC–Variational feedback controller and its application to semi-active suspensions, Mech. Syst. Signal Process. 76 (2016) 72–92, http://dx.doi.org/10.1016/j.ymssp.2016.01.002.

[31] D. Pisarski, A. Myśliński, Online adaptive algorithm for optimal control of structures subjected to travelling loads, Optim. Control Appl. Methods 38 (6) (2017) 1168–1186, http://dx.doi.org/10.1002/oca.2321.

[32] M. Wasilewski, D. Pisarski, Adaptive semi-active control of a beam structure subjected to a moving load traversing with time-varying velocity, J. Sound Vib. 481 (2020) 115404–1–20, http://dx.doi.org/10.1016/j.jsv.2020.115404.

[33] L. Wang, Y. Zhou, S. Nagarajaiah, W. Shi, Bi-directional semi-active tuned mass damper for torsional asymmetric structural seismic response control, Eng. Struct. 294 (2023) 116744, http://dx.doi.org/10.1016/j.engstruct.2023.116744.

[34] D. Lin, F. Yang, D. Gong, R. Li, A new vibration isolator integrating tunable stiffness-damping and active driving properties based on radial-chains magnetorheological elastomer, Mech. Syst. Signal Process. 183 (2023) 109633, http://dx.doi.org/10.1016/j.ymssp.2022.109633.

[35] D. Leng, W. Feng, D. Ning, G. Liu, Analysis and design of a semi-active X-structured vibration isolator with magnetorheological elastomers, Mech. Syst. Signal Process. 181 (2022) 109492, http://dx.doi.org/10.1016/j.ymssp.2022.109492.

[36] Y. Zhao, G. Meng, A bio-inspired semi-active vibration isolator with variable-stiffness dielectric elastomer: Design and modeling, J. Sound Vib. 485 (2020) 115592, http://dx.doi.org/10.1016/j.jsv.2020.115592.

[37] S. Hermann, P. Butaud, R. de O. Teloli, J.-F. Manceau, M. Savary, G. Chevallier, Magnetically induced friction damping based on magnetoactive elastomers — A proof of concept, J. Sound Vib. 534 (2022) 117000, http://dx.doi.org/10.1016/j.jsv.2022.117000.

[38] C. Min, M. Dahlmann, T. Sattel, A concept for semi-active vibration control with a serial-stiffness-switch system, J. Sound Vib. 405 (2017) 234–250, http://dx.doi.org/10.1016/j.jsv.2017.06.007.
[39] D. Pisarski, R. Konowrocki, T. Szmidt, Dynamics and optimal control of an electromagnetically actuated cantilever pipe conveying fluid, J. Sound Vib. 432 (2018) 420–436, http://dx.doi.org/10.1016/j.jsv.2018.06.045.
[40] Y. Hu, T. Hua, M.Z. Chen, S. Shi, Y. Sun, Inherent stability analysis for multibody systems with semi-active inerters, J. Sound Vib. 535 (2022) 117073, http://dx.doi.org/10.1016/j.jsv.2022.117073.
[41] D. Ning, H. Du, N. Zhang, Z. Jia, W. Li, Y. Wang, A semi-active variable equivalent stiffness and inertance device implemented by an electrical network, Mech. Syst. Signal Process. 156 (2021) 107676, http://dx.doi.org/10.1016/j.ymssp.2021.107676.
[42] P. Brzeski, T. Kapitaniak, P. Perlikowski, Novel type of tuned mass damper with inerter which enables changes of inertance, J. Sound Vib. 349 (2015) 56–66, http://dx.doi.org/10.1016/j.jsv.2015.03.035.
[43] S. Lambert-Lacroix, On periodic autoregressive processes estimation, IEEE Trans. Signal Process. 48 (6) (2000) 1800–1803, http://dx.doi.org/10.1109/78.845938.
[44] S. Kay, Modern Spectral Estimation: Theory and Application, Prentice Hall, New York, 1988.
[45] R. Bartels, G.W. Stewart, Solution of the matrix equation AX+XB=C, Commun. ACM 15 (9) (1972) 820–826, http://dx.doi.org/10.1145/361573.361582.
[46] T. Szmidt, D. Pisarski, R. Konowrocki, S. Awietjan, A. Boczkowska, Adaptive damping of a double-beam structure based on magnetorheological elastomer, Shock Vib. 2019 (2019) 8526179–1–16, http://dx.doi.org/10.1155/2019/8526179.
[47] T. Szmidt, D. Pisarski, C. Bajer, B. Dyniewicz, Double-beam cantilever structure with embedded intelligent damping block: Dynamics and control, J. Sound Vib. 401 (2017) 127–138, http://dx.doi.org/10.1016/j.jsv.2017.04.033.

This research was funded in whole or in part by National Science Centre, Poland (grant numbers 2020/39/B/ST8/02615 and 2017/26/D/ST8/00883). For the purpose of Open Access, the authors have applied a CC-BY public copyright licence to any Author Accepted Manuscript (AAM) version arising from this submission.